Structural Engineering and Mechanics, *Vol. 60, No. 5 (2016) 829-849*
DOI: http://dx.doi.org/10.12989/sem.2016.60.5.829

Behaviour of GFRP composite plate under ballistic impact: experimental and FE analyses

Md. Muslim Ansari* and Anupam Chakrabarti[a]

Department of Civil Engineering, Indian Institute of Technology Roorkee, Roorkee-247667, India

(Received May 12, 2016, Revised September 11, 2016, Accepted September 21, 2016)

Abstract. In this paper, experimental as well as numerical analysis of Glass Fiber Reinforced Polymer (GFRP) laminated composite has been presented under ballistic impact with varying projectile nose shapes (conical, ogival and spherical) and incidence velocities. The experimental impact tests on GFRP composite plate reinforced with woven glass fiber (0°/90°)s are performed by using pneumatic gun. A three dimensional finite element model is developed in AUTODYN hydro code to validate the experimental results and to study the ballistic perforation characteristic of the target with different parametric variations. The influence of projectile nose shapes, plate thickness and incidence velocity on the variation of residual velocity, ballistic limit, contact force-time histories, energy absorption, damage pattern and damage area in the composite target have been studied. The material characterization of GFRP composite is carried out as required for the progressive damage analysis of composite. The numerical results from the present FE model in terms of residual velocity, absorbed energy, damage pattern and damage area are having close agreement with the results from the experimental impact tests.

Keywords: GFRP composite; ballistic impact; finite element analyses; projectile nose shape; damage analysis

1. Introduction

FRP composites are versatile materials and used extensively in structural applications due to their virtues of being light in weight, having high stiffness and strength and ease of deployment. Some composite material like GFRP and Kevlar epoxy are resistive against thermal as well as chemical attack in most of the cases and hence these materials are widely used in retrofitting and marine structures like deck harbor, ship decks etc. Due to light weight and high stiffness of FRP composite, these materials are effectively used in the making of indoor and outdoor swimming pools, external body of racing bikes, roof sheeting and bridge deck etc. The laminated composite plate may undergo ballistic impact load, one of the critical load case that the target may encounter during their service condition in the field. Due to orthotropic and non-ductile nature of laminated FRP composite, behaviour of these materials are complicated mainly in terms of damage and its propagation under ballistic impact. The ballistic impact performance of laminated composite target

*Corresponding author, Ph.D., E-mail: muslimdecivil@gmail.com
[a]Professor, E-mail: anupam1965@yahoo.co.uk

http://www.techno-press.org/?journal=sem&subpage=8 ISSN: 1225-4568 (Print), 1598-6217 (Online)

may be affected by various governing parameter like projectile nose shape, target thickness and incidence velocity. Therefore, there is necessity of examining the influence of projectile nose shape and the target thickness on ballistic performance of laminated FRP composite plate especially in terms of perforations and modes of failures.

Numerous researchers have studied the impact behaviour of composite and their works can be classified broadly in three categories such as experimental, numerical and theoretical/analytical. The impact behaviour of composite had been carried out in past by using drop weight test to study the deflection, load transfer and energy absorption (Tiberkak, Bachene *et al*. 2008, Zhang, Sun *et al*. 2013, Evci and Gülgeç 2012, Hossainzadeh 2006). Impact energy was the basis of impact which was governed by head of falling weight and thus the tests were limited for thin plate samples. In the past few years, some attempt had been made to study the penetration behavior of composite laminates. Cantwell and Morton (1989) performed an experimental investigation to study the behavior of CFRP laminate under low and high velocity impact. It was suggested that the elastic deformation, delamination and shear out were the major energy absorbing mechanisms. Nasimuddin and Vaidya (2005) performed an impact analysis of glass/epoxy and graphite/epoxy laminated target. The energy absorption and ballistic limit of the target were studied and it was concluded that the woven glass/epoxy laminate was more damage resistant than the graphite/epoxy laminate. Jordan and Naito (2014) looked at the ballistic and residual velocity of the projectiles impacting on FRP composite plate and concluded that the energy absorbed by the target plate was influenced by the shape of the projectile. Bilingardi and Vadori (2003) analyzed experimentally a glass fiber-epoxy composite plate under low energy impact with small dirt and studied the energy absorption and indentation in composite at different impact energy. Sabet, Fagih *et al*. (2011) worked on high velocity impact performance of glass reinforced polyester (*GRP*) resin with different types of reinforcements and concluded that the shear failure and delamination were dominant in thick composite.

In last two decades, some valuable theoretical investigations on the impact behavior of composite had been reported by researchers. An analytical model was proposed by Landa and Olivares (1995) to study the impact behavior of soft armors. Assumptions made in this analytical model were; perfectly rigid projectile, uniform deceleration of the projectile from one yarn to another and no friction between projectile and the target. Wen (2000, 2001) studied the ballistic limit and residual velocity of the projectile under high velocity impact on FRP composite. It was concluded that the residual velocity of the projectile varied nonlinearly with impact velocity.

After many assumptions and limitations, theoretical investigation was limited for the calculation of residual velocity, ballistic limit and about the energy absorption in most of the cases. To overcome the limitations in impact analysis of composite, numerical approach provides broad aspect of investigation in this regard. Numerically, the damage behaviour in addition to residual velocity and ballistic limit in Kevlar/epoxy composite was studied by some researchers (Kumar, Gupta *et al*. 2010, Tham 2008, Talib, Abbud *et al*. 2012) and the conclusions were drown that the delamination is the major failure in thick composite plate. Recently, Ansari and Chakrabarti (2016) studied the impact behaviour of Kevlar/epoxy composite plate due to low to hyper velocity impact under different parametric variation. It was concluded that the failure in composite plate was localized and being narrower at high projectile velocity.

The review of past studies indicates that the perforation analysis of laminated composite that describes the damage pattern and damage propagation in addition to ballistic limit, residual velocity and energy absorption characteristic of laminated target are still infancy. Moreover, there is scarcity of numerical study available in the literature highlighting the three dimensional progressive damage and modes of failure in laminated composite especially in case of laminated GFRP composite target considering different projectile nose shapes.

The objective of this paper is to study the probable influence of projectile nose shape, target plate thickness and incidence velocity on ballistic perforation behaviour of the laminated composite by experimental as well as finite element analyses.

2. Material, specimens and methods

2.1 Material characterization

To study the damage pattern in laminated FRP composite plate, woven glass fiber lamina $(0°/90°)_s$ has been taken to make laminate by hand layup method. Polyester matrix is applied in such a way that lamina gets wet completely and a nominal pressure is applied to each individual lamina by a soft roller to squeeze out the air voids. The composite laminate is then pressed with a nominal force of 250N. The laminates were further cured in a hot air oven for 3 hours at 80°C to achieve complete solidification (Fig. 1). Specimens of dimension 300 mm×25 mm×10 mm were tested in an Universal Testing Machine (UTM) to determine the elastic properties of the laminated composite (Fig. 2). Specimens dimensioning, manufacturing and testing procedure are followed according to ASTM D3039/D3039M and related literature (AUTODYN manual 2009). The strain gauges of commercial specification "BFLA-5-8" and "FLA-3-8" have been used in longitudinal as well as transverse direction to record the strains in respective directions. The strain gauges are applied nearer to the mid length of the specimens as recommended by ASTM D3039/D3039M, to avoid the readings caused by uneven stress or strain generation in the specimen due to small slippage/adjustment of the jaw of UTM.

Stress-strain curve and longitudinal versus lateral strain curve from the tensile test are shown in Fig. 3. In the coordinate axis system, direction-11 is taken along *z*-direction or through the thickness direction of composite plate, direction-22 and 33 are along *x* and *y* directions or in plane axis of plate according to the direction convention of AUTODYN coordinate system (AUTODYN manual 2012).

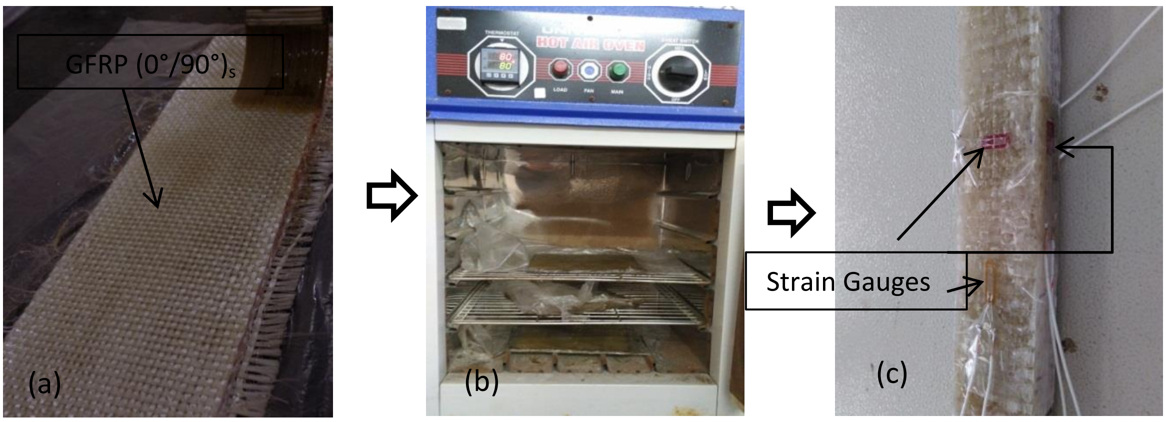

Fig. 1 Processing of GFRP laminate (a) Making laminate by hand layup, (b) Curing in hot air oven, (c) Applying strain gauges in longitudinal and lateral direction

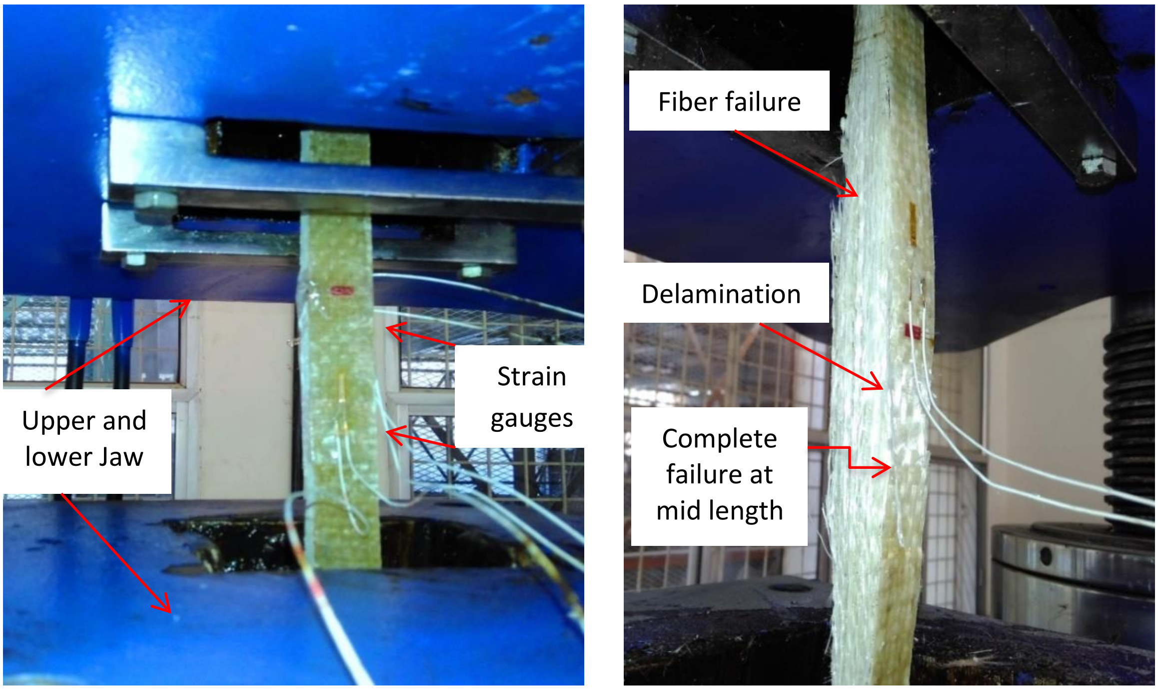

Fig. 2 Tensile test of GFRP for elastic properties in UTM machine

Table 1 Material properties of GFRP and steel 4340 (Johnson and Cook 1985)

GFRP composite	
Equation of state : Orthotropic	Tensile failure Stress 22 (kPa) 4.318e+005
Sub-Equation of State : Polynomial	Maximum Shear Stress 23 (kPa) 8.0e+004
Reference density (gm/cm^3) 1.800	Tensile Failure Strain 11 0.009
Young's modulus 11 (kPa) 6.000e+006	Tensile Failure Strain 22 0.02
Young's modulus 22 (kPa) 1.971e+007	Tensile Failure Strain 33 0.02
Young's modulus 33 (kPa) 1.971e+007	Post Failure Response: Orthotropic
Poisons ratio 12 0.150	Fail 11 & 11 Only
Poisons ratio 23 0.130	Fail 22 &22 Only
Poisons ratio 13 0.150	Fail 33 & 33 Only
Strength : Elastic	Fail 12 & 12 and 11 Only
Shear modulus (kPa) 1.790e+006	Fail 23 & 23 and 11 Only
Failure : Material Stress/Strain	Fail 31 & 31 and 11 Only
	Residual shear Stiff. Frac. 0.20
Steel (4340)	
Equation of States : Linear	Strain rate constant 0.014
Reference density (gm/cm^3) 7.83	Thermal softening exponent 1.04
Bulk modulus (kPa) 1.59E+07	Melting temperature (K) 1793
Reference temperature (K) 300	Failure model : Johnson-Cook
Specific heat capacity (J/kgK) 477	Damage constant, D1: 0.05
Strength :Johnson-Cook	Damage constant, D2: 3.344
Shear modulus (kPa) 7.7E+07	Damage constant, D3: -2.12
Yield Stress (kPa) 7.92E+05	Damage constant, D4: 0.002
Hardening constant (kPa) 5.10E+05	Damage constant, D5: 0.61
Hardening exponent 0.26	

The material properties of GFRP laminated composite as calculated from the present experimental tests are listed in Table 1 along with those available in the material library of AUTODYN for the steel projectile (4340). Out of plane Poison's ratios are calculated from Eqs. (1)-(2) which must hold for the positive stiffness (Silva, Cismaciu *et al*. 2005).

$$|\nu_{12}| = |\nu_{13}| < \left[\frac{E_{11}}{E_{22}}\right]^{1/2}, \qquad |\nu_{23}| < 1 \tag{1}$$

$$\nu_{12}^2 \nu_{23} < \left(1 - \nu_{23}^2\right) \times \left(\frac{E_{11}}{2E_{22}}\right) - \nu_{12}^2 \tag{2}$$

It can be derived from the above relations in conjunction with the material data from Table 1 that the maximum limit of ν_{12} (out of plane Poisson's ratio) is 0.552. A series of high velocity

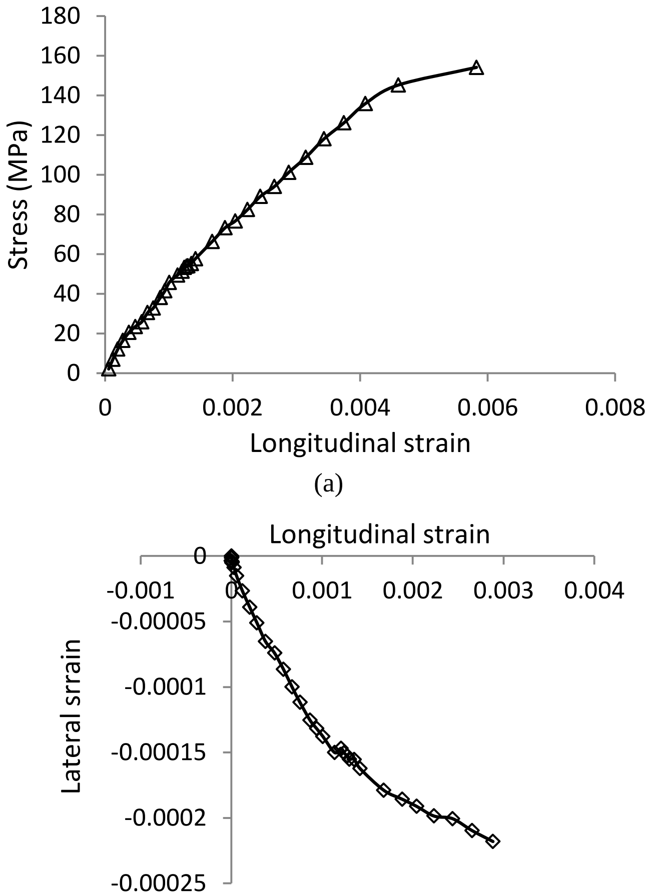

(a)

(b)

Fig. 3 Tensile test on GFRP, (a) Stress-strain curve, (b) Lateral strain vs longitudinal strain for in plane Poison's ratio

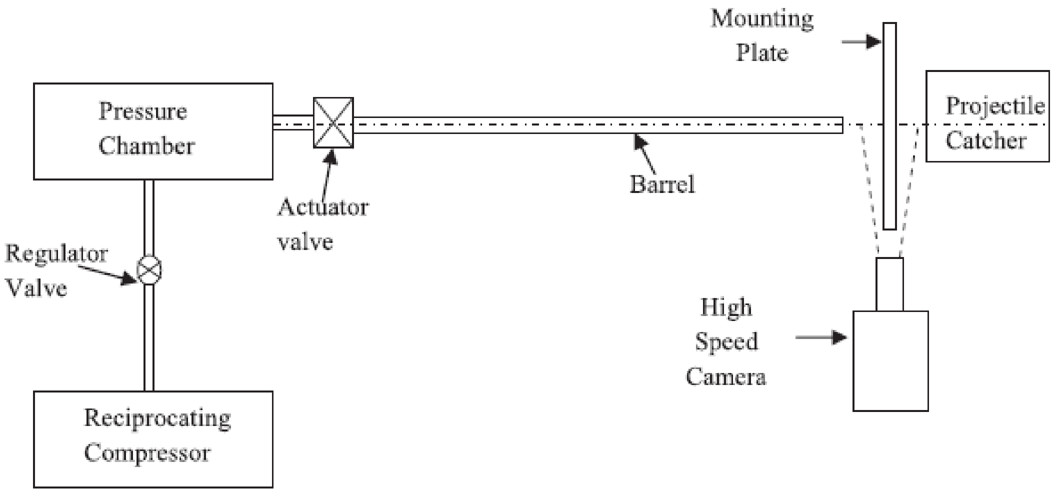

Fig. 4 Schematic diagram of pneumatic gun

impact are performed for the calibration taking the values of v_{12} in between 0 to 0.552. A value of v_{12}=0.15 was found that produced damage pattern in numerical model which matched with the experimental results for all velocity ranges. Ballistic performance is dominated by strength properties of composite plate rather than its stiffness properties (Silva, Cismaciu *et al*. 2005); and this is also confirmed by the ballistic response which shows less sensitivity on this parameter.

2.2 Impact test by Pneumatic gun

Pneumatic gun employed for the impact test in the present experimental work consists of reciprocating compressor, pressure cylinder, an actuator valve and a barrel of varying length depending upon required incidence velocity of projectile. A rigid mounting plate is used to hold the composite target. A high speed framing camera was deployed to record the event which was placed perpendicular to the barrel in line with the mounting plate. A catcher box located behind the mounting plate was used to gather the projectile after perforating the composite plate. The schematic arrangement of the setup is as shown in Fig. 4. The incidence and residual velocities of projectile were measured by using a speed camera “Phantom v411”, The maximum frame rate of the camera was 4200 fps at full resolution (1280×800) and 6, 00,000 fps at the minimum resolution (128×8).

The specimens of composite plate were impacted by cylindrical steel projectile having different nose shapes such as spherical, ogival and conical (Fig. 5(a)). The specimens of composite target plate of dimension 140 mm×140 mm of two different thickness (h=3.12 and 6.24 mm) were made by same procedure as followed during the material characterization. Woven glass fiber lamina was used to make the composite target plate. Five $(0°/90°)_5$ and ten $(0°/90°)_{10}$ laminas were used in same fashion to make laminated composite plates of thickness 3.12 mm and 6.24 mm respectively. Fig. 5(b) show the composite plates with 10 mm diameter holes punched along its four sides to help clamp it along its boundaries.

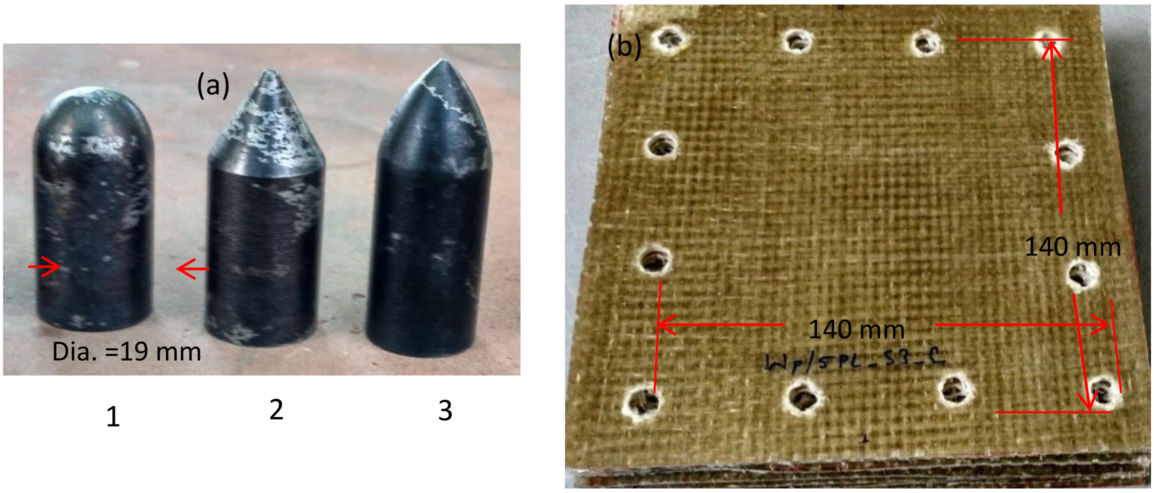

Fig. 5 (a) Projectile nose shapes; 1-spherical, 2-conical, 3-ogival, (b) GFRP composite target plate

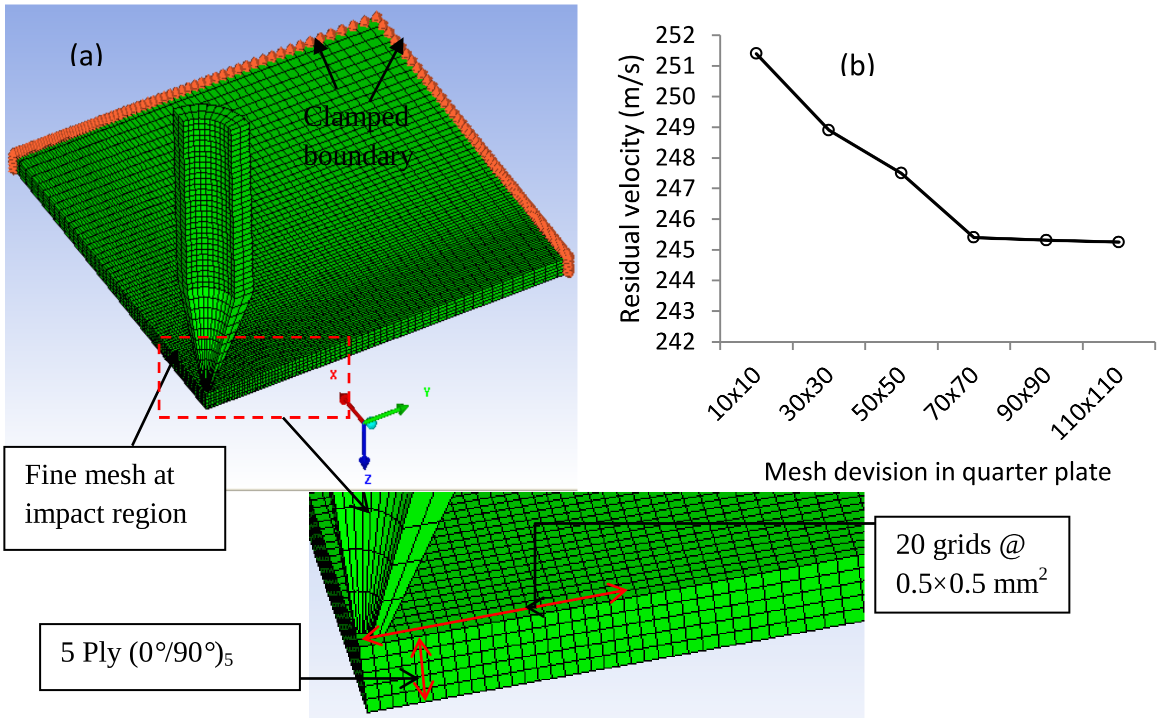

Fig. 6 (a) Numerical model, (b) mesh convergence study (V_i = 274.5 m/s).

3. Numerical and material modeling

3.1 Finite element modeling of target plate and projectile

Numerical simulations provide more insightful understanding of the different modes of failure and their progression as compared to experimentally analyzing failure post mortem after the impact event. In the present study, numerical simulations have been carried out using ANSYS/AUTODYN v14.5, a commercial hydro code. The GFRP composite target plates and the steel projectile with different nose shapes have been modeled using hexahedral brick elements and Lagrangian process.

The contact between projectile and laminate is assumed to be frictionless. Interaction between plate and projectile is defined using gap interaction method with gap size of 0.05 mm (AUTODYN manual 2012). Motion of the projectile is restrained with condition V_x=V_y=0, i.e., the projectile is allowed to move only in *z*-direction. To reduce the computational time only quarter of the target plate is analyzed with symmetric boundary conditions imposed in the plane *X*=0 and *Y*=0. Computational domain for the composite plate is defined in *I*-*J*-*K* space with *I*-MAX=71, *J*-MAX=71 and *K*-MAX varies according to thickness of plate as in experimental test and it is constrained at *I*=71 and *J*=71 planes. Whereas, computational domain for steel projectile in *I*-*J*-*K* space is *I*-MAX=11, *J*-MAZ= 11 and *K*-MAX varies according to shape of projectile nose. A uniform cell size of 0.5 mm is used in both *I* and *J*-directions at impact region as shown in Fig. 6(a). The mesh convergence study has been performed for the composite target plate to find the convergence in the solution (see Fig. 6(b)). A mesh division of 70×70 showed good convergence and was thus used for all the numerical studies. More details about the numerical model and mesh convergence study are discussed in the previous study by Ansari and Chakrabarti (2016).

3.2 Material Modelling of composite plate

The composite plate is modeled as an orthotropic material in AUTODYN hydro v14.5. The through thickness direction-11 is taken along z-axis. For the in-plane properties directions-22 and 33 are along *x* and *y* axes respectively, this convention is similar to what is followed in AUTODYN. All the material properties required for the model are characterized based on the method proposed by Hayhurst, Livingstone *et al*. (2001). The present FE model uses damage model for the orthotropic post failure given by Hayhurst, Livingstone *et al*. (2001) that requires failure stress-strain to calculate fracture energy. Constitutive relations for orthotropic material and nonlinear volumetric response of composite are discussed as below;

EOS (orthotropic)

The incremental linear elastic constitutive relation for orthotropic material can be expressed as

$$\begin{bmatrix} \Delta\sigma_{11} \\ \Delta\sigma_{22} \\ \Delta\sigma_{33} \\ \Delta\tau_{23} \\ \Delta\tau_{31} \\ \Delta\tau_{12} \end{bmatrix} = \begin{bmatrix} C_{11} & C_{12} & C_{13} & 0 & 0 & 0 \\ C_{21} & C_{22} & C_{23} & 0 & 0 & 0 \\ C_{31} & C_{32} & C_{33} & 0 & 0 & 0 \\ 0 & 0 & 0 & C_{44} & 0 & 0 \\ 0 & 0 & 0 & 0 & C_{55} & 0 \\ 0 & 0 & 0 & 0 & 0 & C_{66} \end{bmatrix} \times \begin{bmatrix} \Delta\varepsilon_{11} \\ \Delta\varepsilon_{22} \\ \Delta\varepsilon_{33} \\ \Delta\gamma_{23} \\ \Delta\gamma_{31} \\ \Delta\gamma_{12} \end{bmatrix} \tag{3}$$

In order to include nonlinear shock effects in above equation, it is desirable to separate the volumetric response of material from its ability to resist shear loads. It is convenient to split the strain component into average strain $\Delta\varepsilon_{avg}$ and deviatoric strain $\Delta\varepsilon_{ij}^{d}$. Total strain $\Delta\varepsilon_{ij}$ becomes;

$$\Delta\varepsilon_{ij} = \Delta\varepsilon_{avg} + \Delta\varepsilon_{ij}^{d}$$

Now, average direct strain $\Delta\varepsilon_{avg}$ is defined as one third of trace of strain tensor i.e.

$$\Delta\varepsilon_{avg} = \frac{(\varepsilon_{11} + \varepsilon_{22} + \varepsilon_{33})}{3}$$

For a small strain increment, volumetric strain increment can be defined as

$$\Delta\varepsilon_{vol} \approx \varepsilon_{11} + \varepsilon_{22} + \varepsilon_{33}$$

Orthotropic constitutive relation after total strain increments in terms of volumetric and deviatoric strain can be expressed as

$$\begin{bmatrix} \Delta\sigma_{11} \\ \Delta\sigma_{22} \\ \Delta\sigma_{33} \\ \Delta\tau_{23} \\ \Delta\tau_{31} \\ \Delta\tau_{12} \end{bmatrix} = \begin{bmatrix} C_{11} & C_{12} & C_{13} & 0 & 0 & 0 \\ C_{21} & C_{22} & C_{23} & 0 & 0 & 0 \\ C_{31} & C_{32} & C_{33} & 0 & 0 & 0 \\ 0 & 0 & 0 & C_{44} & 0 & 0 \\ 0 & 0 & 0 & 0 & C_{55} & 0 \\ 0 & 0 & 0 & 0 & 0 & C_{66} \end{bmatrix} \times \begin{bmatrix} \Delta\varepsilon_{11}^{d} + \frac{1}{3}\Delta\varepsilon_{vol} \\ \Delta\varepsilon_{22}^{d} + \frac{1}{3}\Delta\varepsilon_{vol} \\ \Delta\varepsilon_{33}^{d} + \frac{1}{3}\Delta\varepsilon_{vol} \\ \Delta\gamma_{23} \\ \Delta\gamma_{31} \\ \Delta\gamma_{12} \end{bmatrix} \tag{4}$$

The expressions for the direct stress increment can be found out from expanding the above expression and grouping volumetric and deviatoric components as follows

$$\Delta\sigma_{11} = \frac{1}{3}(C_{11} + C_{12} + C_{13})\Delta\varepsilon_{vol} + C_{11}\Delta\varepsilon_{11}^{d} + C_{12}\Delta\varepsilon_{22}^{d} + C_{13}\Delta\varepsilon_{33}^{d}$$

$$\Delta\sigma_{22} = \frac{1}{3}(C_{21} + C_{22} + C_{23})\Delta\varepsilon_{vol} + C_{21}\Delta\varepsilon_{11}^{d} + C_{22}\Delta\varepsilon_{22}^{d} + C_{23}\Delta\varepsilon_{33}^{d}$$

$$\Delta\sigma_{33} = \frac{1}{3}(C_{31} + C_{32} + C_{33})\Delta\varepsilon_{vol} + C_{31}\Delta\varepsilon_{11}^{d} + C_{32}\Delta\varepsilon_{22}^{d} + C_{33}\Delta\varepsilon_{33}^{d} \tag{5}$$

To find the equivalent pressure increment (AUTODYN manual 2012), firstly it can be defined, the pressure as a third of trace of stress increment tensor

$$\Delta P = -\frac{1}{3}(\Delta\sigma_{11} + \Delta\sigma_{22} + \Delta\sigma_{33}) \tag{6}$$

Substituting the Eq. (5) in Eq. (6), contribution to the pressure from volumetric and deviatoric strains can be defined clearly as Eq. (7)

$$\begin{aligned} \Delta P = -\frac{1}{9}[C_{11} + C_{22} + C_{33} + 2(C_{12} + C_{23} + C_{31})]\Delta\varepsilon_{vol} \\ -\frac{1}{3}(C_{11} + C_{21} + C_{31})\Delta\varepsilon_{11}^{d} \end{aligned} \tag{7}$$

$$-\frac{1}{3}(C_{21}+C_{22}+C_{32})\Delta\varepsilon_{22}^{d}$$
$$-\frac{1}{3}(C_{31}+C_{23}+C_{33})\Delta\varepsilon_{33}^{d}$$

From the Eq. (7), first term on the right hand side is used to define volumetric response of orthotropic material in which the effective bulk modulus of the material *K*' is defined as Eq. (8), a function of E_{ij}, υ_{ij} and G_{ij}.

$$K'=\frac{1}{9}[C_{11}+C_{22}+C_{33}+2(C_{12}+C_{23}+C_{31})] \tag{8}$$

Damage Initiation criteria

Target plate and projectile both have been taken as a deformable body. Failure initiation criteria and growth of damage in FRP composite plate is based on the combination of material stress and strain. Hashin failure criteria is used extensively for the modeling and to study the damage in composite due to impact. However, this criterion for matrix and fiber failure is considered only plain stresses σ_{22}, σ_{33} and σ_{23}. Modified version of these failure criteria along with the criteria for delamination has been implemented in AUTODYN. In the fiber failure and matrix cracking, out of plan shear stresses are also considered with original criteria as in Eqs. (9)-(11)

Failure along 11-plane,

$$e_{11f}^{2}=\left(\frac{\sigma_{11}}{\sigma_{11f}}\right)^{2}+\left(\frac{\sigma_{12}}{\sigma_{12f}}\right)^{2}+\left(\frac{\sigma_{31}}{\sigma_{31f}}\right)^{2}\geq 1 \tag{9}$$

Failure along 22-plane,

$$e_{22f}^{2}=\left(\frac{\sigma_{22}}{\sigma_{22f}}\right)^{2}+\left(\frac{\sigma_{12}}{\sigma_{12f}}\right)^{2}+\left(\frac{\sigma_{23}}{\sigma_{23f}}\right)^{2}\geq 1 \tag{10}$$

Failure along 33-plane,

$$e_{33f}^{2}=\left(\frac{\sigma_{33}}{\sigma_{33f}}\right)^{2}+\left(\frac{\sigma_{23}}{\sigma_{23f}}\right)^{2}+\left(\frac{\sigma_{31}}{\sigma_{31f}}\right)^{2}\geq 1 \tag{11}$$

Subsequent to failure initiation, stiffness and strength properties for failed element are changed according to the modes of failure as below.

Delamination: Delamination may occurred due to excessive through thickness tensile stresses and/or strains or from excessive shear stresses and/or strains along 12-plane. If failure initiated in either of these two modes, the stress in 11-direction (through the thickness of the target) is set to be zero instantaneously and strain at failure is stored in 11-direction. Further, if strain in the element exceeds the failure strain, stresses are modified as in Eq. (12)

$$\begin{bmatrix} 0 \\ \Delta\sigma_{22} \\ \Delta\sigma_{33} \\ \Delta\tau_{23} \\ \Delta\tau_{31} \\ \Delta\tau_{12} \end{bmatrix} = \begin{bmatrix} 0 & 0 & 0 & 0 & 0 & 0 \\ 0 & C_{22} & C_{23} & 0 & 0 & 0 \\ 0 & C_{32} & C_{33} & 0 & 0 & 0 \\ 0 & 0 & 0 & \alpha C_{44} & 0 & 0 \\ 0 & 0 & 0 & 0 & \alpha C_{55} & 0 \\ 0 & 0 & 0 & 0 & 0 & \alpha C_{66} \end{bmatrix} \times \begin{bmatrix} \Delta\varepsilon_{11}^{d} + \frac{1}{3}\Delta\varepsilon_{vol} \\ \Delta\varepsilon_{22}^{d} + \frac{1}{3}\Delta\varepsilon_{vol} \\ \Delta\varepsilon_{33}^{d} + \frac{1}{3}\Delta\varepsilon_{vol} \\ \Delta\gamma_{23} \\ \Delta\gamma_{31} \\ \Delta\gamma_{12} \end{bmatrix} \tag{12}$$

In plane failure: In an axisymmetric composite, generally 22 and 33 directions are in the plane. If the failure is initiated in these two modes, stress in the respective direction is set to be zero and this strain is stored as failure strain. If further strain exceeds the failure strain then material stiffness matrix is modified as in Eq. (13)

$$\begin{bmatrix} \Delta\sigma_{11} \\ 0 \\ \Delta\sigma_{33} \\ \Delta\tau_{23} \\ \Delta\tau_{31} \\ \Delta\tau_{12} \end{bmatrix} = \begin{bmatrix} C_{11} & 0 & C_{13} & 0 & 0 & 0 \\ 0 & 0 & 0 & 0 & 0 & 0 \\ C_{31} & 0 & C_{33} & 0 & 0 & 0 \\ 0 & 0 & 0 & \alpha C_{44} & 0 & 0 \\ 0 & 0 & 0 & 0 & \alpha C_{55} & 0 \\ 0 & 0 & 0 & 0 & 0 & \alpha C_{66} \end{bmatrix} \times \begin{bmatrix} \Delta\varepsilon_{11}^{d} + \frac{1}{3}\Delta\varepsilon_{vol} \\ \Delta\varepsilon_{22}^{d} + \frac{1}{3}\Delta\varepsilon_{vol} \\ \Delta\varepsilon_{33}^{d} + \frac{1}{3}\Delta\varepsilon_{vol} \\ \Delta\gamma_{23} \\ \Delta\gamma_{31} \\ \Delta\gamma_{12} \end{bmatrix} \tag{13}$$

Eq. (13) represents the stiffness matrix after failure in 22-direction and similar expressions are used for the failure along 33-direction. In practice, 20% is typically used for the residual shear stiffness fraction (α) in the analysis.

4. Results and discussions

Fig. 7 shows the variation in residual velocity (V_r) with incidence velocity (V_i) for different composite target plates (h=6.24 mm and 3.12 mm) and projectiles (nose shapes: conical, ogival and spherical) from both experimental and numerical analysis. The variation in residual velocity appears to be similar for different projectiles as considered. The numerical results from FE analysis also show close agreement with experimental results. The laminated GFRP composite plate of size 140 mm×140 mm having thicknesses 6.24 mm and 3.12 mm were impacted by 52 g cylindrical steel projectile of diameter 19 mm. All the four edges of plate were firmly clamped with sample holder.

The ballistic limit of the target plate under projectile impact is defined as the minimum incidence velocity at which projectile perforates the target completely. The ballistic limit velocity

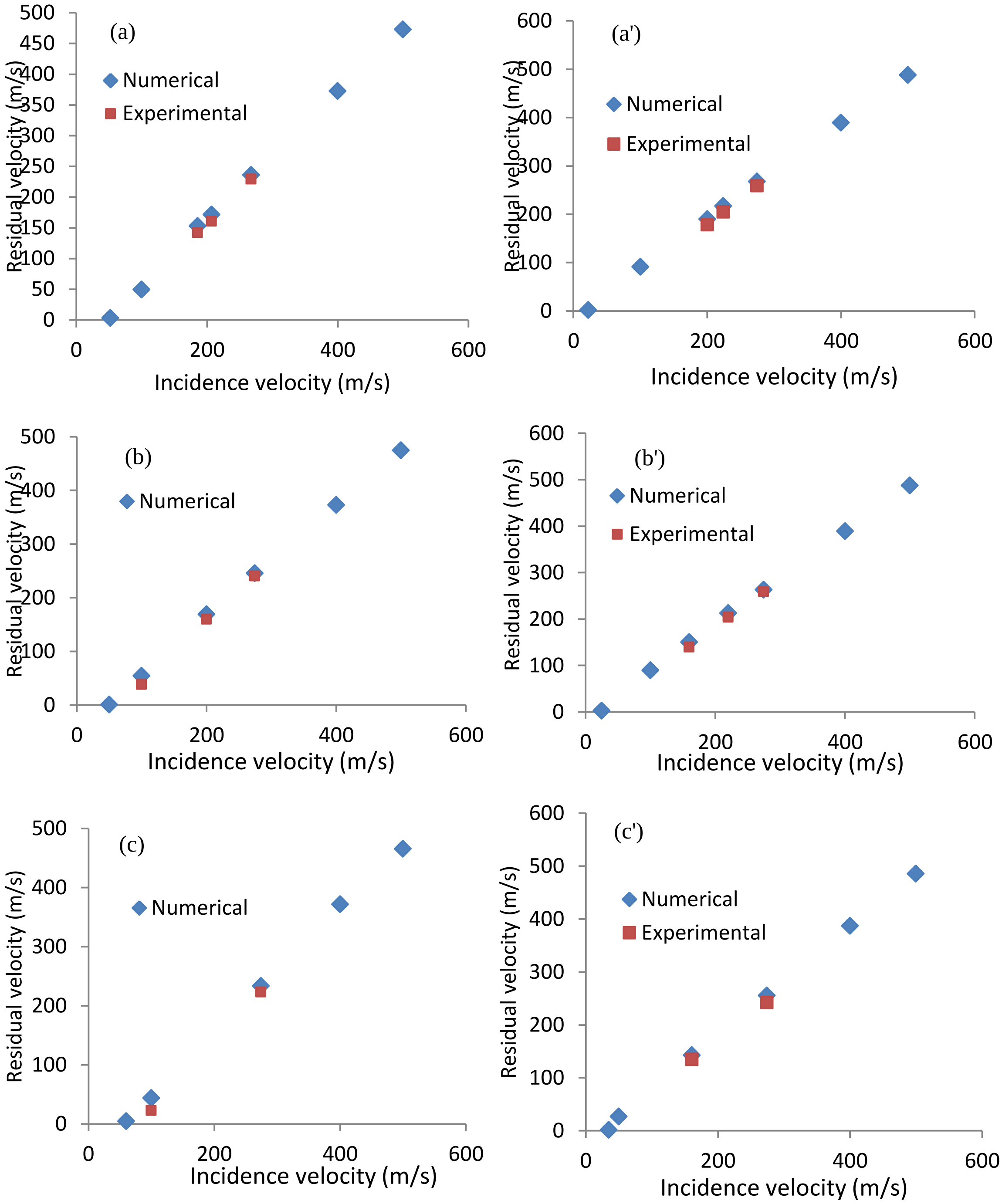

Fig. 7 Variation of V_r with V_i; (a) Conical nosed projectile, *h*=6.24 mm, (b) Ogival nosed projectile, *h*=6.24 mm, (c) Spherical nosed projectile, *h*=6.24 mm, (a') Conical nosed projectile, *h*=3.12 mm, (b') Ogival nosed projectile, *h*=3.12 mm, (c') Spherical nosed projectile, *h*=3.12 mm

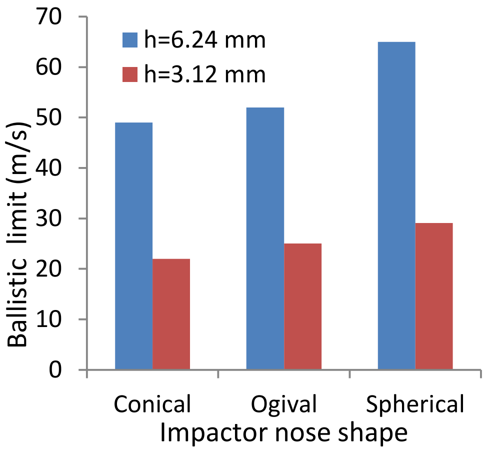

Fig. 8 Variation of ballistic limit for projectiles of different nose shapes

(a)

(b)

(c)

(d)

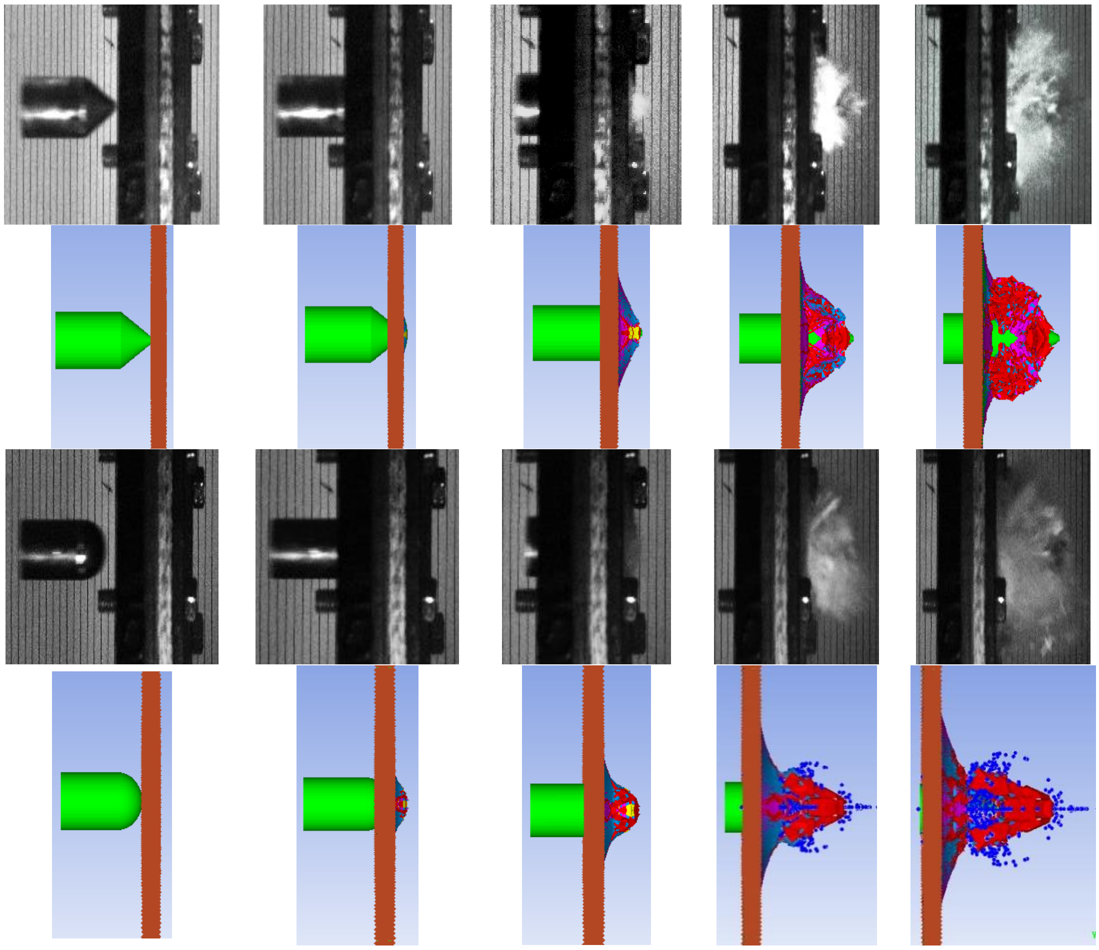

Fig. 9 Penetration/perforation of FRP composite plate by projectiles at different time frame; (a) Exp. by conical nosed projectile, (b) Num. by conical nosed projectile, (c) Exp. by spherical nosed projectile, (d) Num. by spherical nosed projectile

of the target demonstrates the perforation resistance offered by the target plate to the projectile. The ballistic limits (V_b) of 3.12 and 6.24 mm thick target plates have been presented with varied projectile nose shapes (conical, ogival and spherical), see Fig. 8. The ballistic limit of 6.24 mm thick target increases from 49.0 to 65 m/s with the projectile nose shape changes from conical to spherical. It means the ballistic limit increased by 16 m/s. However, this increase in the ballistic limit of 3.12 mm thick target is found to be 7.1 m/s. This shows that the perforation behavior of thick composite target is more influenced by projectile nose shape as compared to thin composite target.

Fig. 9 shows the penetration process of the composite plate of thickness 6.24 mm at different time frames by the conical and spherical projectile with incidence velocity of 274.5 m/s. It is observed that the bulk mass of the target bulge out around the conical nosed projectile with clear exit of conical nose. This is due to the fact that the fibers of the lamina displaced from the impact point as the conical nosed projectile tried to pierce through, Fig. 9(b). However, rupture of the fibers takes place in the laminate due to excessive tension in case of spherical nosed projectile impact which is caused due to more contact surface area. Thus more amount of plug is generated and ejected followed by projectile, Fig. 9(d). Plug formation on the back face of composite plate is observed from both experimental and numerical simulation for the projectiles.

To study the progressive damage modes and their variation with different nose shapes of projectile, composite target plates of size 140 mm×140 mm×6.24 mm are impacted by projectiles of different nose shapes (ogival and spherical) at incidence velocity of 274.5 m/s. Fig. 10 shows the cross sectional view of composite plate and projectile at different time frame. As the projectile starts to penetrate inside the composite plate, the delamination starts first near impact region. The induced delamination in the composite target is found to be more in case of impact by spherically nosed projectile as compared to ogival nosed projectile, Figs. 10(b) and (b'). This may due to the fact that the spherical nosed projectile offers more impact force with more contact surface area as compared to ogival nosed projectile

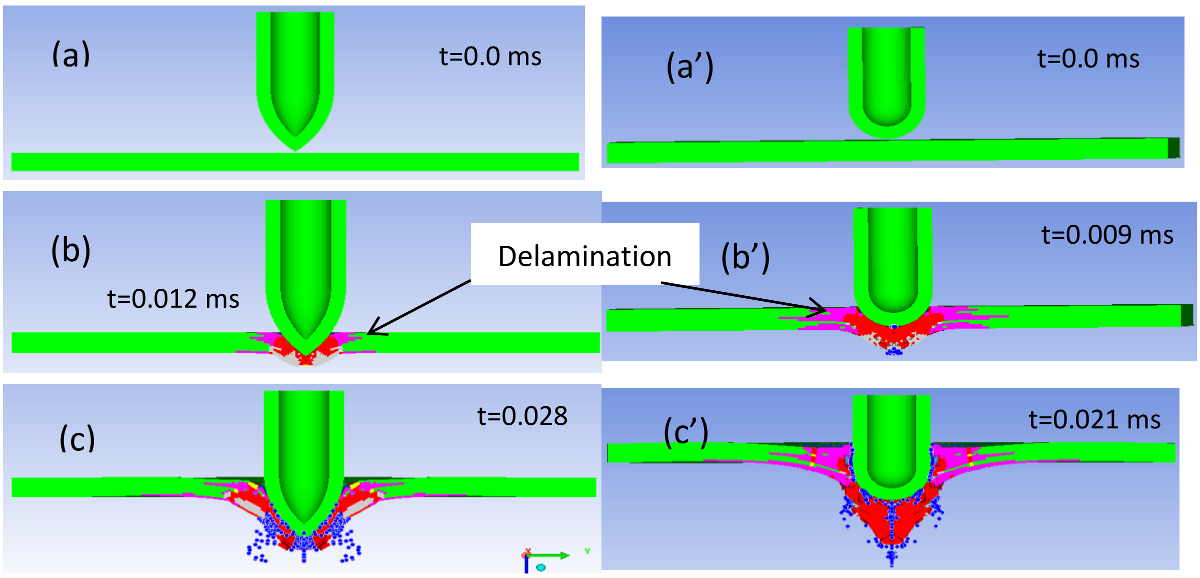

Fig. 10 Different modes of damage evolution at different time frame

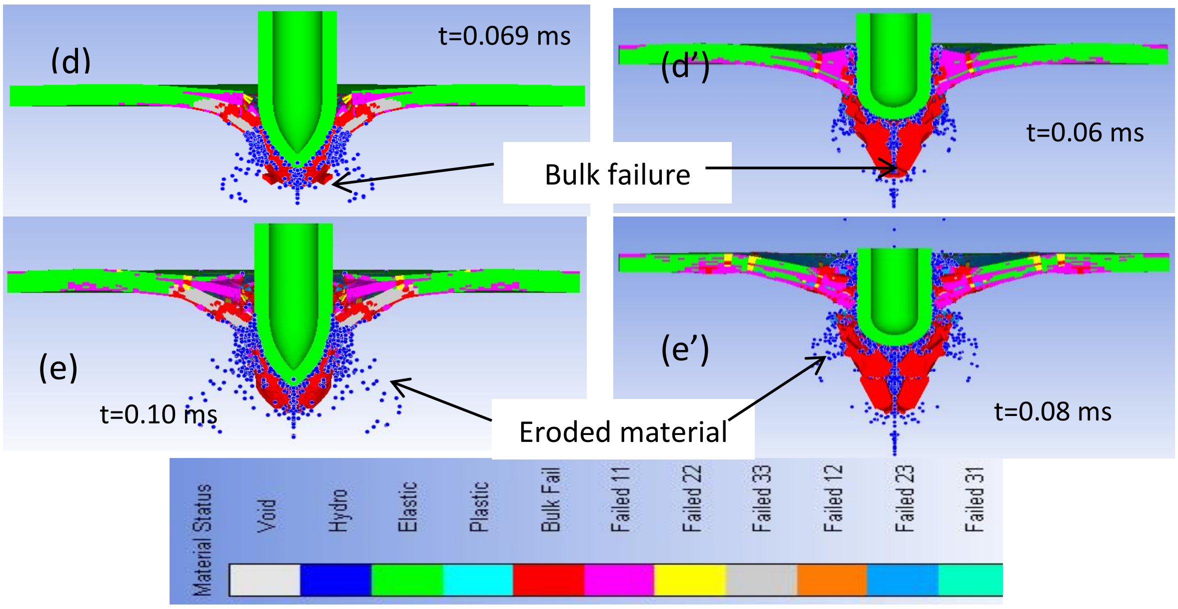

Fig. 10 Continued

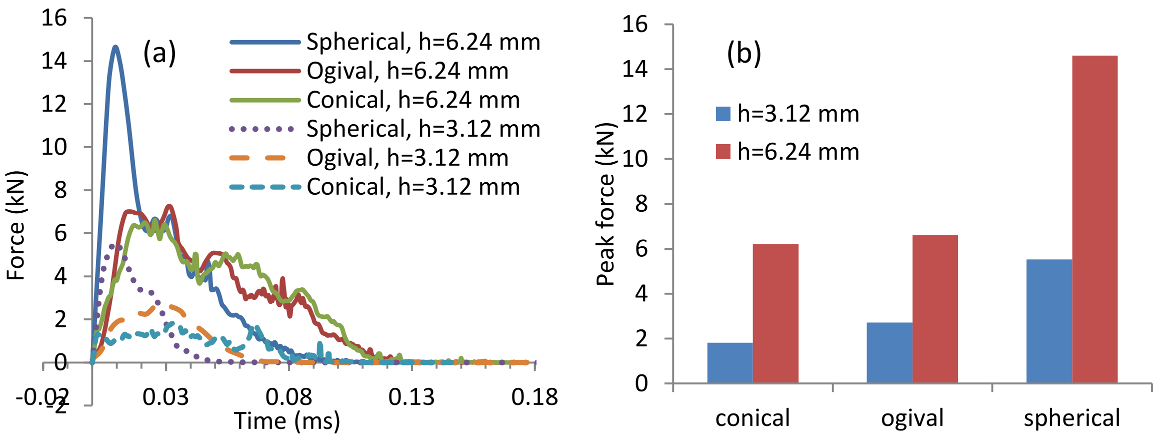

Fig. 11 (a) Force-time histories for projectiles of different nose shapes, (b) Variation of peak force with projectile nose shapes

Bulk failure in composite plate represents complete failure or breakage of fiber along with matrix. Failure of matrix occurs mainly due to tension and thus matrix failure is predicted by failed-11, failed-23 and failed-12 or 13 as shown in material status bar from the present FE model. Bulk failure occurs in the composite plate just beneath the projectile and the amount of failure is more in the case of spherical nosed projectile in comparison with the ogival projectile, see Figs. 10(d) and (d'). This is also observed from Fig. 10 that the overall damaged length is more in case of impact by spherical nosed projectile than ogival projectile.

With the present numerical model; the ballistic impact behaviour of composite target plate in terms of contact force-time histories has also been studied with varying projectile nose shapes and composite target thickness (h=3.12 and 6.24 mm). It is observed that the peak value of contact force in the target occurs at different time for projectiles having different nose shapes. The occurrence time of peak force is found to be 0.009 ms for spherical nosed projectile as shown in Fig. 11(a). It means that, the maximum impact energy imparted by spherical nosed projectile is up to time 0.009 ms however, the time of occurrence of peak force in 3.12 mm thick target lies in between 0.02 to 0.035 ms for ogival and conical nosed projectiles. Moreover, the force-time history becomes narrower as the projectile nose shape changes from conical to spherical. This is due to increase in the contact surface of the projectiles.

The peak value of contact force in 6.24 mm thick target is also observed to be increased from 6.21 kN for conical to 14.6 kN for spherical nosed projectile. However the peak force of 3.2 mm thick target is increased by 3.71 kN with the projectile nose shape changes from conical to spherical. From the above observations, it is found that the time of occurrence and magnitude of peak force decreases with thickness of the target.

The loss of kinetic energy of the projectile is assumed to be absorbed in composite plate that causes failure of plate, Eq. (14).

$$E_{abs} = m \times (V_i^2 - V_r^2) / 2 \tag{14}$$

Where, E_{abs} is absorbed energy in the composite plate. m, V_i and V_r are mass, incidence velocity and residual velocity of the projectile respectively.

Fig. 12 shows the effect of projectile nose shape and thickness of composite plate on the energy absorption. The composite plate appears to absorb more energy when impacted by the spherical nosed projectile compared to that of the ogival nose shaped projectile. The energy absorption in composite plate increases as the thickness of plate increases. It is also observed that, the energy absorption is more in experimental impact test than the result obtained from the numerical analysis in most of the cases. This difference may be due to the friction that acts between projectile and composite plate during penetration. It is to be noted that in the present numerical model,

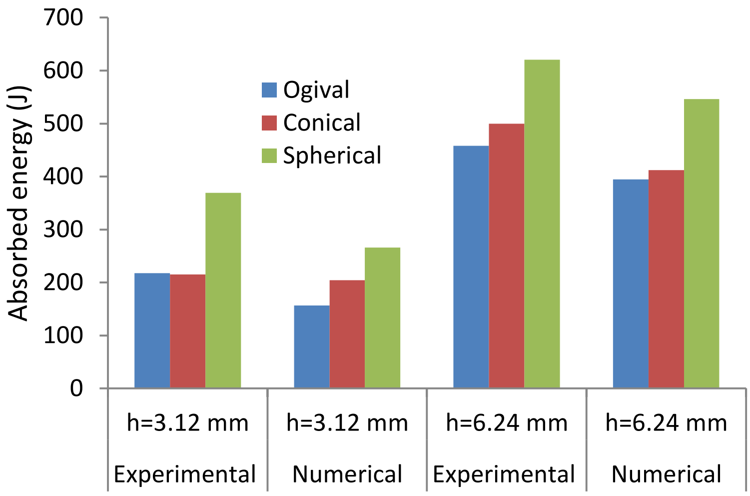

Fig. 12 Energy absorbed in composite plate due to impact by projectile of different nose shape with incidence velocity 274.5 m/s

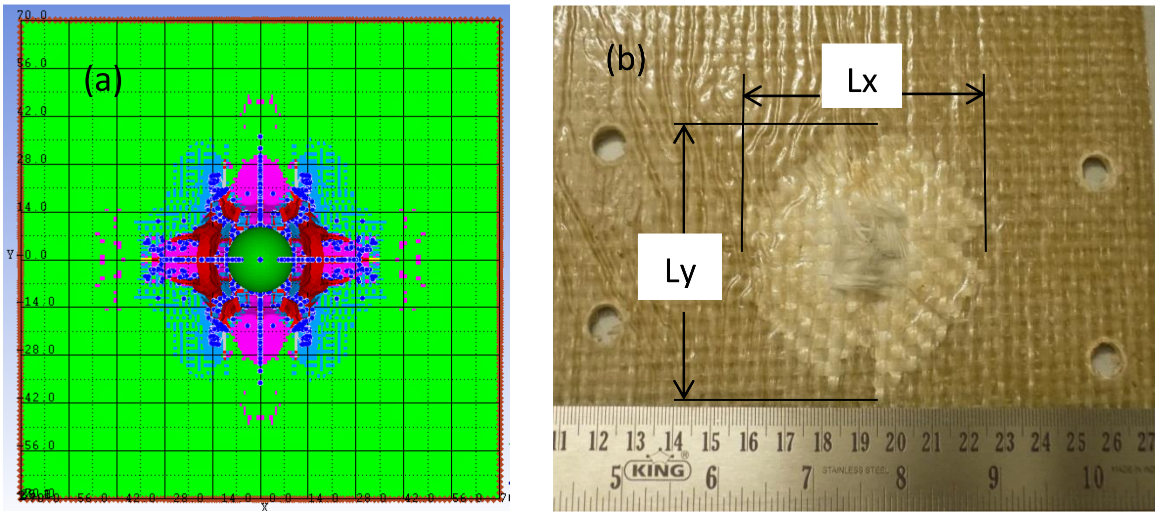

Fig. 13 Measurement of damaged length on back face of composite plate with scale

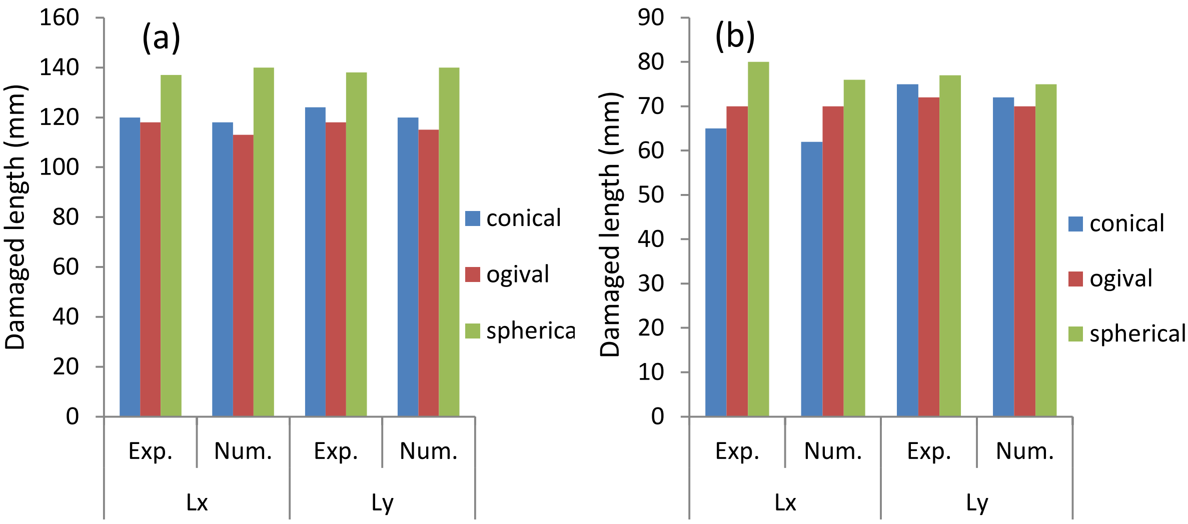

Fig. 14 Variation of damaged length with projectile nose shape, (a) *h*=6.24 mm, (b) *h*=3.12 mm

frictionless contact is defined between projectile and composite plate.

Damage in GFRP composite plates is not circular in shape and therefore it is characterized in terms of its lengths measured along *x* and *y* directions. Fig. 13 compares the damage pattern and magnitude of the thin composite plate from the experiments and numerical analysis for the ogival nosed projectile having an initial velocity of at 274.5 m/s. In the numerical model (Fig. 13(a)) each small grid is of length of 7 mm and Fig. 13(b) shows the back face of tested specimen with measuring scale and a typical representation of damaged length in *x* and *y* directions.

Fig. 14 shows the effect of projectile nose shapes (at V_i =274.5 m/s) on the damage lengths (or damaged area) along *x* and *y* directions for the two different plate thickness (*h*=3.12 mm and 6.24 mm). It is seen that the damaged length is more in case of impact with the spherical nosed

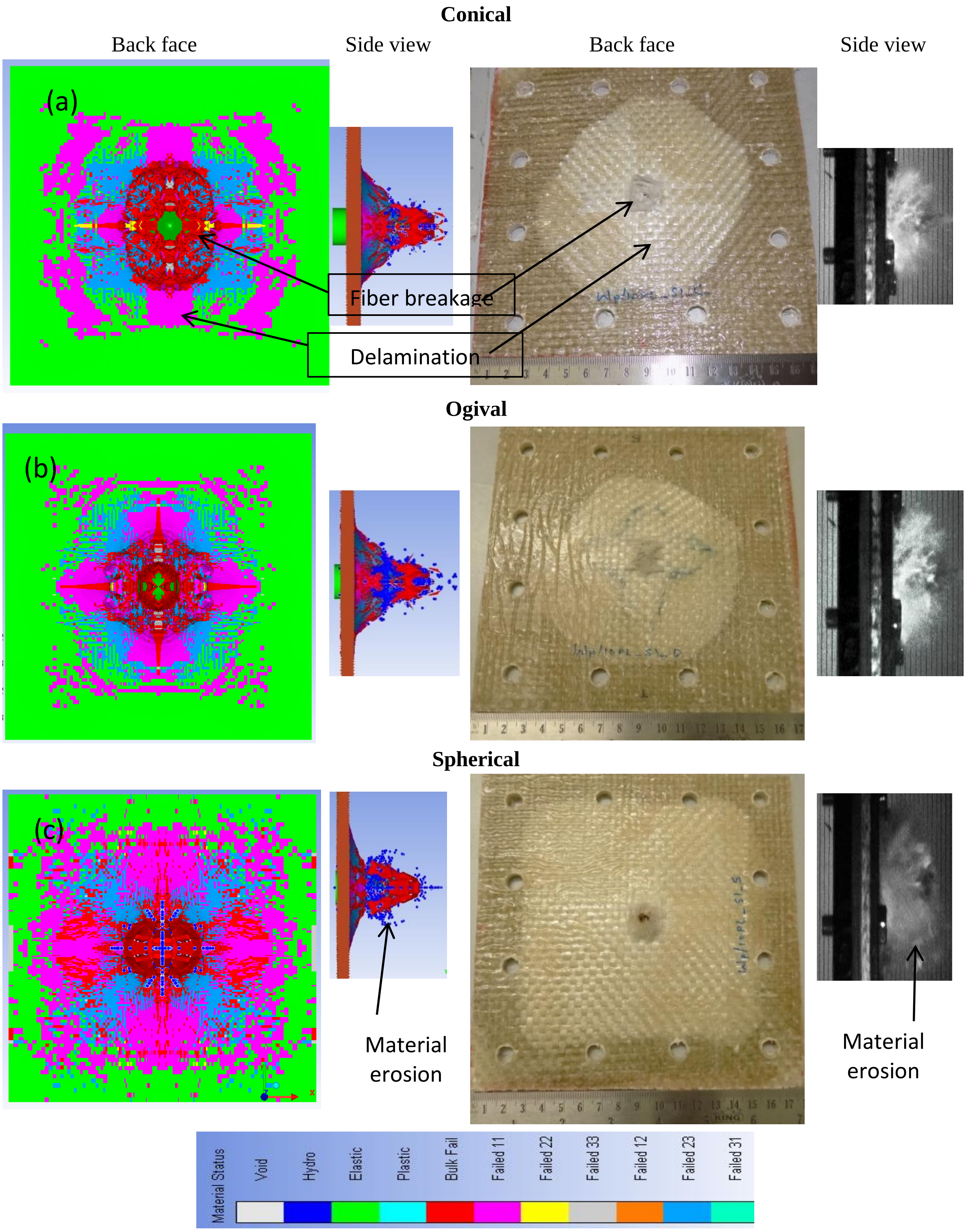

Fig. 15 Damage pattern in composite plate under ballistic impact with incidence velocity 274.5 m/s

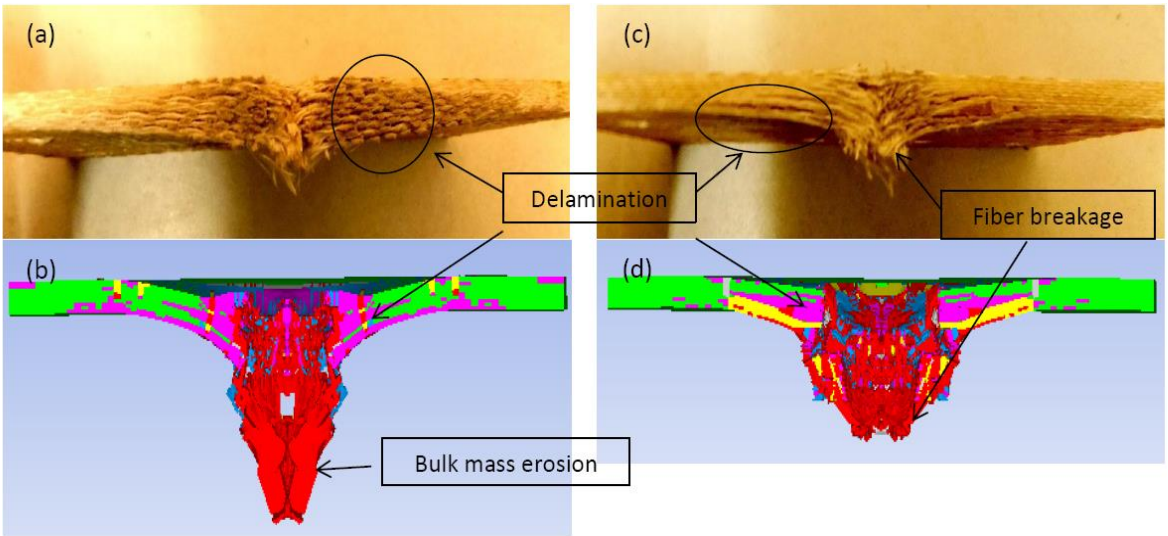

Fig. 16 Cross sectional view of damage pattern in GFRP composite plate from Exp. and Num. results, (a, b) sperical nosed projectile, (c, d) conical nosed projectile

projectile for both plate thicknesses. This may be due to the fact that more energy is absorbed for a spherical nosed projectile (see Fig. 12). Both numerical and experimental results show that the conical projectile creates more damage in the 6.24 mm thick plate as compared to the ogival projectile. For ogival and spherical nosed projectiles, differences in damaged length along x and y axis are 19 mm and 20 mm from experimental test and 23 mm and 25 mm from numerical model for plate thickness 6.24 mm. Whereas, this differences in the damaged length along x and y axis are 10 mm and 6 mm from experimental test and 5 mm and 5 mm from numerical model for the plate of thickness 3.12 mm. It may be concluded from this observation that, the effect of projectile nose shape on the damage length in laminated FRP composite plate due to ballistic impact is more in case of thick plate than thinner one.

Damage Pattern as observed in FRP composite plates due to ballistic impact from the experimental and numerical results are compared in Fig 15. It is seen that delamination forms a major component of damage. Delamination of fiber is predominant that comes just under projectile nose and this delamination makes a plus like shape on the back face of composite plate as shown in Fig. 15(a) as may be observed in both numerical and experimental test. Causes and its quantitative representation of delamination can be studied with numerical model effectively than experimental test. From Figs. 15(a and c) and material failure status bar of the numerical model of AUTODYN, it is observed that most of the delaminated area occurs due to matrix failure (i.e., delamination along the thickness i.e. in 11- direction) as shown in pink colour.

Some part of delamination also may be due to in plane failure as indicated by “Failed 23”, Breakage of fiber also occurs just below projectile nose. As the projectile is fired above the ballistic limit, materials from composite plate gets eroded and are seen coming out from the back face of plate (Fig. 15(c)).

Fig. 16 shows the cross-sectional view of damage pattern in laminated GFRP composite plate (h=6.24 mm) due to impact by spherical and conical nosed projectile at V_i=274.5 m/s. it is observed that all the constituting laminas are delaminated near the impact region in case of impact by spherical nosed projectile compared to conical projectile impact. In case of impact by conical nosed projectile, delamination is predominant near the back face of composite plate as shown in Fig. 16(c). Bulk mass of composite material is eroded from the plate in case of impact by spherical nosed projectile compared to conical projectile as shown in Figs. 16(b and d).

5. Conclusions

Ballistic impact behavior of laminated GFRP composite plate has been investigated in the present study. Detailed experimental as well as numerical study has been carried out to study the damage behavior and the probable influence of projectiles having different nose shapes. The effects of target thickness and projectile shapes on the damage, energy absorption, contact force-time histories and ballistic limit have been presented. Modes of failure and their progression due to ballistic impact have also been studied for two different shapes of projectiles (spherical and ogival). Experimental and numerical analysis showing penetration and consequently the plug formation on back face of the composite target due to conical and spherical projectiles has also been presented. Composite material has been characterized based on ASTM D3039/D3039M specification. Results from the numerical analysis should be useful for researchers working in the field. Some important observations from the present study are summarized below;

Ballistic impact behavior of GFRP composite plate in terms of ballistic limit, variation of residual velocity, energy absorption, contact force and failure pattern are found to be influenced by projectile nose shapes as well as plate thickness.

The ballistic limit velocity for the composite target plate increases as the projectile nose shape change from conical to spherical.

The trend of variation of residual velocity is almost similar but their magnitudes are different for all the projectiles having different nose shapes.

Peak value of contact force occurs earlier in case of projectile having spherical nose shape.

Energy absorption in composite plate is more when it was impacted by spherical ended projectile than the others. Also, the effect of projectile nose shape on energy absorption is less for thinner composite plate.

Damaged area in composite plate is more in case of ballistic impact by projectile having more contact surface (spherical projectile) irrespective of incidence velocity. Damage in thick composite plate is more influenced by projectile nose shape as compared to thin plate.

Damage in the composite plate due to ballistic impact is predominantly due to delamination and this occurs mainly due to matrix failure in tension. Some parts of delaminated surface are also caused by in-plane failure rather than matrix failure.

Fiber breakage occurs just beneath the projectile nose. Also, the breakage of fiber is more in case of projectile having more contact surface area (spherical).

References

Ansari, M.M. and Chakrabarti, A. (2016), "Impact behaviour of FRP composite plate under low to hyper velocity impact", *Compos. Part B*, **95**, 462-474.

Ansari, M.M. and Chakrabarti, A. (2016), "Progressive damage of GFRP composite plate under ballistic impact: experimental and numerical study", *Polymer Polymer Compos*., **24**(7), 579-586.

ANSYS/AUTODYN 14.5 (2012), User's manual, ANSYS Inc. South Pointe.
Bilingardi. G. and Vadori, R. (2003), "Influence of the laminate thickness in low velocity impact behavior of composite material plate", *Compos. Struct*., **61**, 27-38.
Cantwell, W.J. and Morton, J. (1989), "A comparison of the low and high velocity impact response of CFRP", *Compos*., **20**(6), 545-551.
Evci, C. and Gülgeç, M. (2012), "An experimental investigation on the impact response of composite materials", *Int. J. Impact. Eng*., **43**, 40-51.
Hayhurst, C.J., Livingstone, I.H.G., Clegg, R.A. *et al*. (2001), "Ballistic limit evaluation of advanced shielding using numerical simulations", *Int. J. Impact Eng*., **26**, 309-320.
Hossainzadeh, R., Shokrieh, M.M. and Lessard, L. (2006), "Damage behavior of fiber reinforced composite plates subjected to drop weight impacts", *Compos. Sci. Tech.*, **66**(1), 61-68.
Johnson, G.R. and Cook, W.H. (1985), "Fracture characteristics of three metals subjected to various strains, strains rates, temperature and pressure", *Eng. Frac. Mech*., **21**, 31-48.
Jordan, J.B. and Naito, C.J. (2014), "An experimental investigation of the effect of nose shape on fragments penetrating GFRP", *Int. J. Impact Eng*., **63**, 63-71.
Kumar, S., Gupta, D.S., Singh, I. and Sharma, A. (2010), "Behavior of Kevlar/Epoxy Composite Plates under Ballistic Impact", *J. Rein. Plast. Compos*., **29**, 2048-2064.
Landa, B.P. and Olivers, F.H. (1995). "An analytical model to predict impact behavior of soft armor", *Int. J. Impact Eng*., **16**, 455-466.
Nasimuddin, P.E. and Vaidya, U. (2005), "Ballistic testing of polymer composites to manufacture emergency safe house shelters", *J. Compos. Constr*., **9**(4), 369-375.
Sabet, A., Fagih, N. and Beheshty, M.H. (2011), "Effect of reinforcement type on high velocity impact response of GRP plates using a sharp tip projectile", *Int. J. Impact Eng.*, **38**, 715-722.
Silva, M.A.G., Cismaciu, C. and Chiorean, C.G. (2005), "Numerical simulation of ballistic impact on composite laminates", *Int. J. Impact Eng*., **31**, 289-306.
Talib, A.R.A., Abbud, L.H., Ali, A. and Mustapha, F. (2012), "Ballistic impact performance of Kevlar-29 and Al_2O_3 powder/epoxy targets under high velocity impact", *Mater. Des*., **35**, 12-29.
Tham, C.Y., Tan, V.B.C. and Lee, H.P. (2008), "Ballistic impact of a Kevlar helmet: experimental and simulations", *Int. J. Impact Eng*., **35**, 304-318.
Tiberkak, R., Bachene, M., Rechak, S. and Necib, B. (2008), "Damage prediction in composite plates subjected to low velocity impact", *Compos. Struct.*, **83**, 73-82.
Wen, H.M. (2000), "Predicting the penetration and perforation of FRP laminates struck normally by projectiles with different nose shapes", *Compos. Struct*., **49**, 321-329.
Wen, H.M. (2001), "Penetration and perforation of thick FRP laminates", *Compos. Sci. Tech*., **61**, 1163-1172.
Zhang, D., Sun, Y., Chen, L. and Pan, N. (2013), "A comparative study on low-velocity impact response of fabric composite laminates", *Mater. Des*., **50**, 750-756.

CC

Notations

C_{ij}	-	stiffness coefficient in *i, j* direction
h	-	thickness of composite plate
V_i	-	incidence velocity of projectile
V_r	-	residual velocity of projectile
V_b	-	ballistic limit velocity of projectile